2011-06-15

Using Lagrangian Coherent Structures to Study Coastal Water Quality

Laura A. Fiorentino
University of Miami, lauraannf@gmail.com

UNIVERSITY OF MIAMI

USING LAGRANGIAN COHERENT STRUCTURES TO STUDY COASTAL WATER QUALITY

By

Laura Ann Fiorentino

A THESIS

Submitted to the Faculty
of the University of Miami
in partial fulfillment of the requirements for
the degree of Master of Science

Coral Gables, Florida

June 2011

UNIVERSITY OF MIAMI

A thesis submitted in partial fulfillment of
the requirements for the degree of
Master of Science

USING LAGRANGIAN COHERENT STRUCTURES TO STUDY COASTAL WATER QUALITY

Laura Ann Fiorentino

Approved:

_____
Maria J. Olascoaga, Ph.D.
Professor of Applied Marine Physics

_____
Terri A. Scandura, Ph.D.
Dean of the Graduate School

_____
Michael G. Brown, Ph.D.
Professor of Applied Marine Physics

_____
Adrianus Reniers, Ph.D.
Professor of Applied Marine Physics

_____
Helena Solo-Gabriele, Ph.D.
Professor of Civil, Architectural
and Environmental Engineering

FIORENTINO, LAURA ANN (M.S., Applied Marine Physics)
Using Lagrangian Coherent Structures (June 2011)
To Study Coastal Water

Abstract of a thesis at the University of Miami.

Thesis supervised by Professor Maria J. Olascoaga.
No. of pages in text. (29)

In order to understand water quality in the coastal ocean and its effects on human health, the necessity arises to locate the sources of contaminants and track their transport throughout the ocean. Dynamical systems methods are applied to the study of transport of enterococci as an indicator of microbial concentration in the vicinity of Hobie Beach, an urban, subtropical beach in Miami, FL that is used for recreation and bathing on a daily basis. Previous studies on water quality have shown that Hobie Beach has high microbial levels despite having no known point source. To investigate the cause of these high microbial levels, a combination of measured surface drifter trajectories and numerically simulated flows in the vicinity of Hobie Beach is used. The numerically simulated flows are used to identify Lagrangian Coherent Structures (LCSs), which provide a template for transport in the study area. Surface drifter trajectories are shown to be consistent with the simulated flows and the LCS structure. LCSs are then used to explain the persistent water contamination and unusually high concentrations of microbes in the water off of this beach as compared with its neighboring beaches. From the drifter simulations, as well as field experiments, one can see that passive tracers are trapped in the area along the coastline by LCS. The Lagrangian circulation of Hobie Beach, influenced primarily by tide and land geometry causes a high retention rate of water near the shore, and can be used to explain the elevated levels of enterococci in the water.

TABLE OF CONTENTS

LIST OF FIGURES

Figure

Chapter 1: Introduction

Hobie Beach, located in Biscayne Bay, in Miami, FL (figure 1), is a popular recreational beach in a subtropical urban environment, whose appeal is continually marred by sub-standard water quality. The beach attracts large crowds of visitors due to its proximity to downtown Miami, free parking, and the fact that dogs are allowed. There are several similar beaches located near this beach, but only Hobie Beach has been chosen due to the greater number of exceedences in indicator bacteria levels as compared to other beaches in Miami-Dade County and the fact that it has been studied extensively for hazards to human health. As part of the Florida Healthy Beaches Program, the water is regularly tested for the enterococci, a fecal indicator bacteria, whose presence indicates contamination from human waste. Hobie Beach, which has no known point sources of pollution, is often put under swim advisories for exceeding the EPA Poor Water Quality Guideline for enterococci and is the subject of several studies designed to uncover the sources of pollutants and an explanation for the beach's high microbe levels (Wright et al., 2009; Shibata et al., 2004).

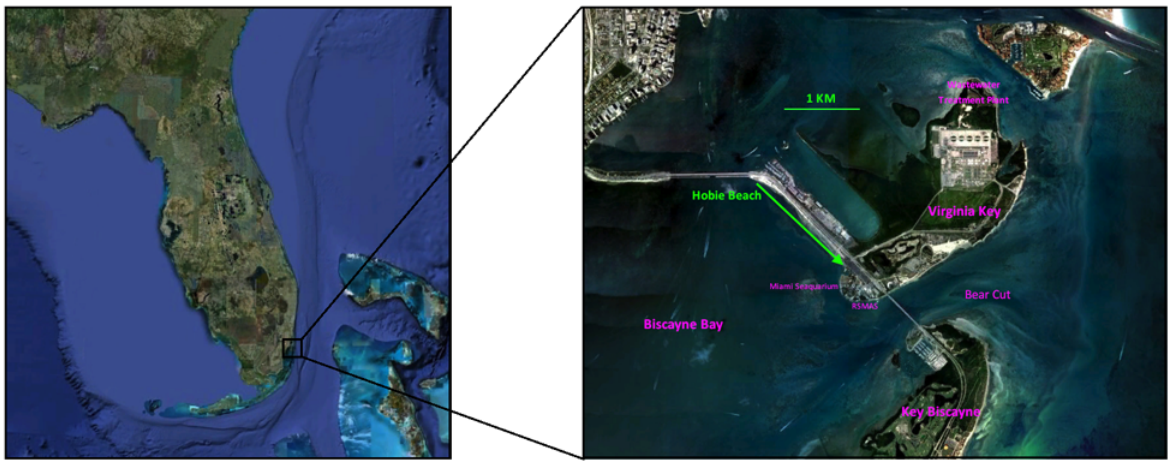

Figure 1: Hobie Beach, located in Biscayne Bay, in Miami, FL

The sands in the intertidal zone and wash zone were shown to be the predominant locus of enterococci's highest concentration (Shibata et al., 2004). Recent studies on

the influence of animal feces, including those of dogs, seagulls, and shrimp mounds (Wright et al., 2009), as well as human shedding (Elmir et al., 2007), on the bacteria content in the sand and water have shown that, while these are significant contributors to the elevated levels (Zhu et al., 2011), they are not enough to account for the measured enterococci concentration levels. This disparity between known sources of contamination and levels of bacteria suggests that other mechanisms are at play that contribute to the elevated enterococci concentration along the shoreline of Hobie Beach. One likely mechanism is the Lagrangian circulation in the vicinity, which possibly favors the accumulation of pollutants released along the shoreline, thereby contributing to elevate the levels of enterococci concentration at Hobie Beach. The Lagrangian circulation in the vicinity of Hobi Beach is studies here using dynamical systems methods.

The particular dynamical systems concept considered is that of the (hyperbolic) Lagrangian Coherent Structure or LCS. Motivated by the observation of the emergence of organized patterns in the distribution of a tracer (e.g., a pollutant) that is passively advected by a time-dependent velocity field, a physical definition of an LCS has been given by Haller and Yuan (2000), and recently formalized in precise mathematical terms by Haller (2011). Specifically, an LCS can be physically defined as a locally strongest repelling or attracting material fluid surface. Attracting and repelling LCSs act as the core material surfaces responsible for stretching and folding, respectively, in a passive tracer. Repelling (attracting) LCSs are like the stable (unstable) manifolds of hyperbolic trajectories in autonomous flows, e.g., (Ottino, 1990; Wiggins, 1992). Because LCSs are the building blocks of the skeleton of the Lagrangian circulation, revealing LCSs facilitates the interpretation of time-dependent velocity records, as well as helps predict the evolution of a passive tracer.

The remainder of the thesis has the following organization: In Chapter 2, a description of the site being studied is given, as well as a background on the mathematical

techniques used throughout the thesis. Chapter 3 provides the methods and results of computational experimentation, and methods and results of field experimentation are then given in chapter 4. Finally, the conclusions and future work are presented in chapter 5.

Chapter 2: Background

2.1 Site Description

Hobie Beach is located on Virginia Key, which is in Biscayne Bay, east of mainland Miami. The beach is situated 35 m from and parallel to the Rickenbacker Causeway, which connects Virginia Key to downtown Miami. It is approximately 1.6 km long and, on average, 5 m wide. The average ambient temperature for the area is 24.8° C and the average annual precipitation is 152.6 cm (Shibata et al., 2004). The dominant tidal component is the M_2 semidiurnal principal lunar tidal component, which has a period of approximately 12.421 hours (Apel, 1987). The tidal amplitude ranges from .6 m to .9 m throughout the year. Tidal data is obtained from NOAA's coastal tide station on Virginia Key (http://tidesandcurrents.noaa.gov/geo.shtml?location=8723214).

Hobie Beach has no known point source of pollution, an observation that has led to much interest and study of this beach. The Miami Dade County Central Waste Water Treatment Plant is located on the northern part of the key, but studies have shown that its outfall, which is about 3.25-km into the Atlantic Ocean, and other remote sources do not affect the enterococci levels at Hobie Beach (Shibata et al., 2004). Directly adjacent to the site beach is the Miami Seaquarium, a marine animal amusement park. The water from its animal tanks is chlorinated before being discharged, so this is not considered to be a source of microbial pollution. There are no storm drains that discharge water into the beach, and the nearest river is about 2 km north.

One unique feature of Hobie Beach is that patrons are permitted to bring their dogs. As there are no lifeguards or any form of authority on the beach, more often than not, animal waste is not cleaned up. One study, aimed to determine the microbial load from animal feces at Hobie Beach, compared the enterococci concentrations in feces from dogs, birds, and shrimp mounds, as well as those from human bather

shedding. The study concludes that dogs are a large contributing source to the microbe concentrations on the beach (Wright et al., 2009). Though, the limited spatial extent of the enterococci plume from dog waste has lead others to determine that there must be others sources of microbes (Zhu, 2009). Without a distinct cause for waste to exist in the water, there is no clear way to keep the beach clean.

2.2 Lagrangian Coherent Structures

The use of dynamical systems methods and examination of flow from a Lagrangian perspective can aid in the study of mixing and transport of passive tracers in the ocean. From the Lagrangian approach, one studies fluid motion by examining particle trajectories, as opposed to the Eulerian view, where one focuses on velocities at fixed locations in space. Particle trajectories are given by $\mathbf{x}(t; \mathbf{x}_0, t_0)$, the solutions to the nonautonomous dynamical system

$$\dot{\mathbf{x}} = \mathbf{u}(\mathbf{x}, t) \tag{1}$$

where $\mathbf{u}$ is the smooth velocity field of the fluid defined over a finite-time interval $t \in [t_0, t_0 + \tau]$ and in the open domain U. The flow map for the system, $\mathbf{F}_{t_0}^{t}(\mathbf{x}_0)$, maps the initial position $\mathbf{x}_0$ to its position at time t:

$$\mathbf{F}_{t_0}^{t} : U \to U \tag{2}$$

$$\mathbf{x}_0 \mapsto \mathbf{x}(t; \mathbf{x_0}, t_0) \tag{3}$$

When taking the Lagrangian approach, one important component to investigate is the behavior of ensembles of trajectories. Codimension-one sets of trajectories are the most significant of these ensembles because they divide distinct regions, between

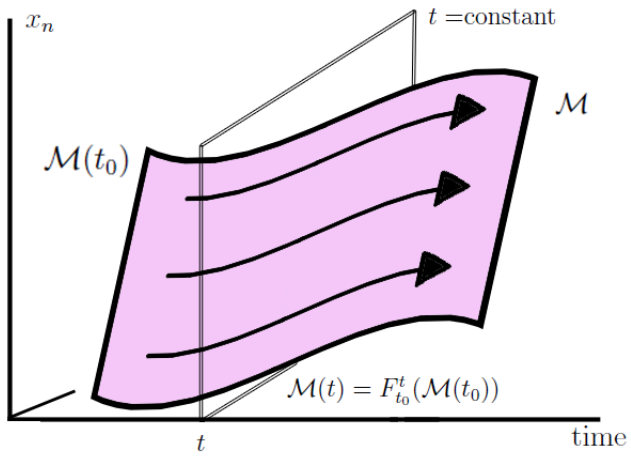

Figure 2: Material surface $\mathcal{M}(t)$ generated in the extended phase space by the flow map from a surface $\mathcal{M}(t_0)$ of initial conditions. Adapted from (Haller, 2011)

which no transport exists. These sets of trajectories are invariant manifolds. And a material surface $\mathcal{M}(t)$, shown in Figure 2, is the t =const slice of the codimension-one invariant manifold $\mathcal{M}$ in the extended phase space generated by the advection of an $(n-1)$-dimensional surface of initial conditions $\mathcal{M}(t_0)$ by the flow map $\mathbf{F}_{t_0}^{t}$.

A Lagrangian Coherent Structure (LCS), is defined by Haller (2011) as "a locally strongest repelling or attracting material surface over" a finite time interval, that act as skeletons of patterns formed by trajectories. An illustration of this concept is shown in Figure 3. One tool that can be used to find LCSs is the Finite Time Lyapunov Exponents (FTLE). An FTLE is a measure of the largest particle separation rate. To calculate an FTLE, we look at the infinitesimal perturbation ξ to the trajectory $\mathbf{x}(t; \mathbf{x_0}, t_0)$. At time t, the perturbation evolves to:

$$\nabla \mathbf{F}_{t_0}^{t_0+\tau}(\mathbf{x}_0)\xi, \tag{4}$$

where $\nabla \mathbf{F}_{t_0}^{t_0+\tau}(\mathbf{x}_0)$ is the deformation gradient. The largest stretching along the trajectory is given by the maximum value of the deformation gradient:

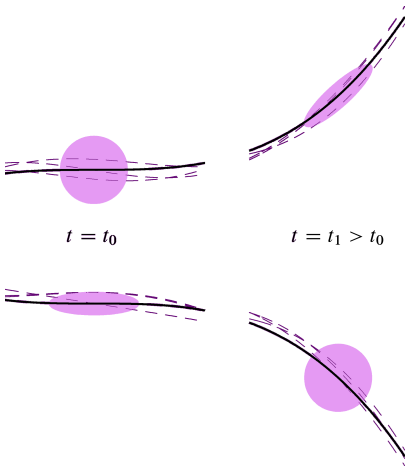

Figure 3: An attracting LCS (top panel) over the finite-time interval $[t_0, t_1]$ is locally the strongest attracting material fluid surface among all nearby material fluid surfaces. A sphere of initially nearby fluid particles at $t = t_0$ will deform such that the attracting LCS will acts its centerpiece at $t = t_1$. A repelling LCS (bottom panel) is an attracting LCS in backward time, $[t_1, t_0]$.

$$\max_{\boldsymbol{\eta}\neq 0} \frac{\|\boldsymbol{\nabla}\mathbf{F}_{t_0}^{t_0+\tau}(\mathbf{x}_0)\boldsymbol{\xi}\|}{\|\boldsymbol{\eta}\|} = \|\boldsymbol{\nabla}\mathbf{F}_{t_0}^{t_0+\tau}(\mathbf{x}_0)\| \tag{5}$$

$$= \sqrt{\lambda_{\max}[\boldsymbol{\nabla}\mathbf{F}_{t_0}^{t_0+\tau}(\mathbf{x}_0)^{\mathrm{T}}\boldsymbol{\nabla}\mathbf{F}_{t_0}^{t_0+\tau}(\mathbf{x}_0)]} \tag{6}$$

$$= \sqrt{\lambda_{\max}[\mathbf{C}_{t_0}^{t_0+\tau}(\mathbf{x}_0)]} \tag{7}$$

where $\lambda_{\max}$ is the maximum eigenvalue and

$$\mathbf{C}_{t_0}^{t_0+\tau}(\mathbf{x}_0) = \boldsymbol{\nabla}\mathbf{F}_{t_0}^{t_0+\tau}(\mathbf{x}_0)^{\mathrm{T}}\boldsymbol{\nabla}\mathbf{F}_{t_0}^{t_0+\tau}(\mathbf{x}_0) \tag{8}$$

is the finite-time Cauchy-Green strain tensor. The FTLE is defined as

$$\Lambda_{t_0}^{\tau}(\mathbf{x}_0) := \|2\tau\|^{-1} \ln \lambda_{\max}[\mathbf{C}_{t_0}^{t_0+\tau}(\mathbf{x}_0)], \tag{9}$$

$\Lambda_{t_0}^{\tau}(\mathbf{x}_0)$ is a forward time FTLE when $\tau > 0$, and a backward time FTLE when $\tau < 0$. Shadden et al. (2005) shows that the finite time Lyapunov exponent is Lagrangian in

the limit of large integration times T, because it is derived from particle trajectories and becomes constant along trajectories for times T.

While Haller (2011) has recently shown that the ridges of FTLE fields do not necessarily mark LCSs, they are still often useful in revealing LCSs (Shadden et al., 2005; Olascoaga et al., 2006; Lekien, 2007). In order to determine the relevance of the FTLE fields for the identification of LCSs, Haller (2011) developed a variational theory of LCSs. Specifically, let $(\lambda_i(\mathbf{x}_0, t_0, \tau), \boldsymbol{\xi}_i(\mathbf{x}_0, t_0, \tau))$ be an eigenvalue–eigenvector pair for $\mathbf{C}_{t_0}^{t_0+\tau}(\mathbf{x}_0)$, i.e.,

$$\mathbf{C}_{t_0}^{t_0+\tau}(\mathbf{x}_0)\boldsymbol{\xi}_i(\mathbf{x}_0, t_0, \tau) = \lambda_i(\mathbf{x}_0, t_0, \tau)\boldsymbol{\xi}_i(\mathbf{x}_0, t_0, \tau). \tag{10}$$

Because $\mathbf{C}_{t_0}^{t_0+\tau}(\mathbf{x}_0)$ is symmetric and positive-definite, $\lambda_i(\mathbf{x}_0, t_0, \tau) \in \mathbb{R}^+$ and $\{\boldsymbol{\xi}_i(\mathbf{x}_0, t_0, \tau)\}$ forms an orthogonal basis. Assume that $\{\boldsymbol{\xi}_i(\mathbf{x}_0, t_0, \tau)\}$ have been appropriately normalized and consider the ordering

$$0 < \lambda_1(\mathbf{x}_0, t_0, \tau) \leq \cdots \leq \lambda_{n-1}(\mathbf{x}_0, t_0, \tau) \leq \lambda_n(\mathbf{x}_0, t_0, \tau). \tag{11}$$

Then Haller (2011) demonstrated that sufficient conditions for an FTLE ridge to mark an LCS are the following:

1. $\lambda_{n-1} \neq \lambda_n > 1$;

2. $\boldsymbol{\xi}_n$ is orthogonal to the FTLE ridge;

3. the matrix

$$\mathbf{L} = \begin{pmatrix} \nabla\nabla\mathbf{C}^{-1}\left(\xi_n\xi_n\xi_n\xi_n\right) & 2\frac{\lambda_n-\lambda_1}{\lambda_1\lambda_n}\xi_1\cdot\nabla\xi_n\xi_n & \cdots & 2\frac{\lambda_n-\lambda_{n-1}}{\lambda_{n-1}\lambda_n}\xi_{n-1}\cdot\nabla\xi_n\xi_n \\ 2\frac{\lambda_n-\lambda_1}{\lambda_1\lambda_n}\xi_1\cdot\nabla\xi_n\xi_n & \frac{2\lambda_n-\lambda_1}{\lambda_1\lambda_n} & \cdots & 0 \\ \vdots & \vdots & \ddots & \vdots \\ 2\frac{\lambda_n-\lambda_{n-1}}{\lambda_{n-1}\lambda_n}\xi_{n-1}\cdot\nabla\xi_n\xi_n & 0 & \cdots & \frac{2\lambda_n-\lambda_{n-1}}{\lambda_{n-1}\lambda_n} \end{pmatrix}$$

where

$$\nabla\nabla\mathbf{C}^{-1}\left(\xi_n\xi_n\xi_n\xi_n\right) = -\frac{1}{\lambda_n^2}\xi_n\cdot\nabla^2\lambda_n\xi_n + 2\sum_1^{n-1}\frac{\lambda_n-\lambda_i}{\lambda_i\lambda_n}\left(\xi_i\cdot\nabla\xi_n\xi_n\right)^2 \qquad (12)$$

is positive definite.

Haller (2011) further showed that a sufficient condition for the robustness of an LCS marked by an FTLE ridge under small perturbations of the flow map $\mathbf{F}_{t_0}^{t_0+\tau}$ is

4. $\boldsymbol{\xi}_n\cdot\nabla\nabla\lambda_n\boldsymbol{\xi} + \boldsymbol{\nabla}\lambda_n\cdot\boldsymbol{\nabla}\boldsymbol{\xi}_n\boldsymbol{\xi}_n < 0$.

Chapter 3: Computational Methods

3.1 CAFE3D Model

The hydrodynamic model used to produce the surface velocity fields for this study is CAFE3D, a finite element model based on the vertically integrated equations of motion, forced by winds, tides and canal discharges (Wang, 1978; Wang and van de Kreeke, 1986; Wang et al., 1994). In order to obtain a sufficiently small resolution and accurately represent the shallow water, Wang used a finite element model, in contrast to previous finite difference models that were restricted by a square grid. The governing equations in the model are the vertically integrated continuity and momentum equations:

$$\frac{\partial \eta}{\partial t} + \frac{\partial Hu}{\partial x} + \frac{\partial Hv}{\partial y} = 0 \tag{13}$$

$$\frac{\partial u}{\partial t} + u\frac{\partial u}{\partial x} + v\frac{\partial u}{\partial y} - fv = -g\frac{\partial \eta}{\partial x} + A_l\left(\frac{\partial^2 u}{\partial x^2} + \frac{\partial^2 u}{\partial y^2}\right) + \frac{A_z}{H}\frac{\partial u}{\partial z}\Big|_{\zeta} - \frac{A_z}{H}\frac{\partial u}{\partial z}\Big|_{-h} \tag{14}$$

$$\frac{\partial v}{\partial t} + u\frac{\partial v}{\partial x} + v\frac{\partial v}{\partial y} + fu = -g\frac{\partial \eta}{\partial y} + A_l\left(\frac{\partial^2 v}{\partial x^2} + \frac{\partial^2 v}{\partial y^2}\right) + \frac{A_z}{H}\frac{\partial v}{\partial z}\Big|_{\zeta} - \frac{A_z}{H}\frac{\partial v}{\partial z}\Big|_{-h} \tag{15}$$

where u and v are the vertically averaged velocities; h is the water depth; η is the water surface elevation; $H = h+\eta$; A_l is the horizontal eddy viscosity; and A_z is the vertical eddy viscosity. Several assumptions were used to obtain equations [1-3]. The fluid is assumed to be incompressible, $\nabla \cdot \mathbf{u} = 0$. The hydrostatic approximation, and $\frac{\partial p}{\partial z} = \rho g$ the Boussinesq approximation, in which density variations are negligible outside the gravity term, are applied. Reynolds averaging, in which turbulence is simplified by decomposing the flow into mean and fluctuating parts, $u = \bar{u} + u'$, and then time averaged. Molecular diffusion is neglected, and turbulent diffusion is parameterized

in analogy to molecular diffusion, using a Fick's Law type of relationship:

$$\overline{u'u'} = 2A_l \frac{\partial u}{\partial x} \qquad \overline{v'v'} = 2A_l \frac{\partial v}{\partial y} \tag{16}$$

$$\overline{u'v'} = A_l \left(\frac{\partial u}{\partial y} + \frac{\partial v}{\partial x} \right) \qquad \overline{u'w'} = A_z \frac{\partial u}{\partial z} \tag{17}$$

The surface boundary conditions are given by the wind stress,

$$\tau_{wind} = \rho_a C_D U_{10}^2, \tag{18}$$

where ρ_a is the air density, U_{10} is the wind speed at 10 m, and C_D is the drag coefficient:

$$\begin{aligned} C_D &= (0.49 + 0.065 * U_{10}) * 0.001 && U_{10} > 11 \frac{m}{s} \\ C_D &= 1.2 * 0.001 && U_{10} < 11 \frac{m}{s} \end{aligned} \tag{19}$$

The bottom friction is obtained from the Manning formula for steady uniform flow in an open channel or gravity-driven free surface flow:

$$V = \frac{1}{n} R^{2/3} S^{1/2}, \tag{20}$$

where V is the cross-sectional average velocity, R is the hydraulic radius, S is the slope of the water surface, and n is the Manning roughness coefficient. For this model n= .025 (Streeter, 1961; Zhu, 2009).

The flows normal to the model's land boundaries are zero. The surface elevation is used for the open boundaries. Along the north and west open boundaries, the surface elevations are a sum of different tidal components, the tidal amplitude and phases based on the Virginia Key Station tidal components. The data for

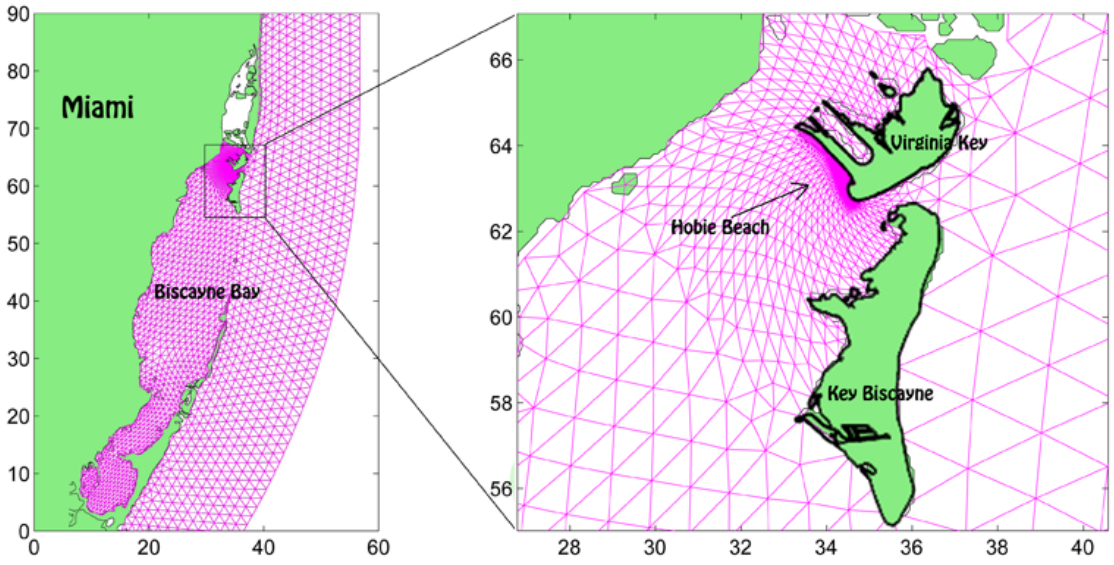

Figure 4: Finite element numerical grid used for the CAFE3D model.

the model topography is from the NOAA nautical chart 11451. The hourly wind data is obtained from the National Marine Buoy Center station at Virginia Key (http://www.ndbc.noaa.gov/station_page.php?station=vakf1). The station is located at 25.732 N 80.162 W, 3m above mean sea level. The anemometer is located 10.28 m above the site elevation, or 13.28 m above the mean sea surface level. Figure 5 shows the hourly wind velocity for April 19th 2011. The main component of fluid motion in this area of the bay is due to tidal forcing. The dominant tidal component is the M2 semidiurnal, principal lunar tidal mode, which has a period of $T = 12.421$ hours. Hobie Beach has a mean tidal range of 0.616 m., average depth of 3 m, average velocity around .05 m/s and weak circulation due to the shape of the land at either end (Zhu, 2009; Wang, 1978; Wang and van de Kreeke, 1986). The tidal forcing, shallow depths, and land shape all have an impact on the coastal circulation.

The original CAFE3D model covers an area that is approximately 65 km wide and 160 km long, with very low resolution near Hobie Beach. For a previous study that also focused on Hobie Beach, the model was improved (Zhu, 2009). Originally, the grid size is approximately 600m at Hobie Beach, consisting of only two of the

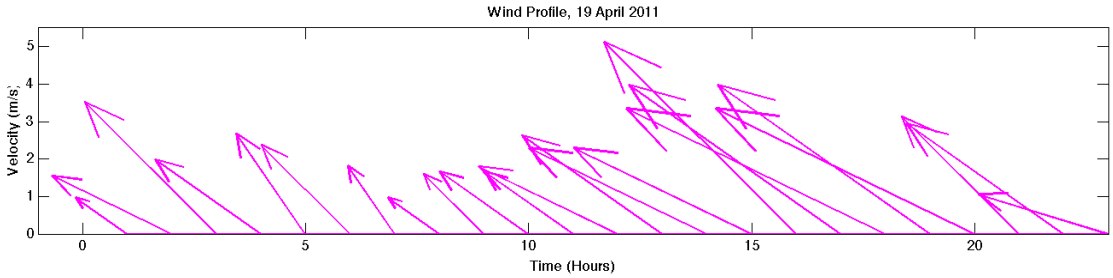

Figure 5: Wind profile for April 19th 2011

triangular finite elements. The refined model grid now has a resolution of 15 m near the coastline of Hobie Beach and up to 1600m outside of Biscayne Bay. Also, the grid was expanded to include the sub-basin between the Rickenbacker Causeway and the Port of Miami, Bear Cut inlet, and the embayment northwest of Virginia Key (Zhu, 2009; Zhu et al., 2011). The model grid, which now contains 2905 grid points and 5294 triangular elements, is shown in figure 4. For use in this thesis the model was enhanced by Ad Reniers. The time step was decreased in order to increase stability, some boundary conditions were changed to provide higher resolution areas around Hobie Beach.

3.2 FTLE Computation

While the CAFE3D model used a triangular grid to increase resolution, it was necessary to interpolate the velocity fields into a regular grid in order to use software that calculates FTLE fields. After testing several interpolation methods, Matlab's TriScatteredInterp function with natural neighbor interpolation was chosen as the most accurate for this task. Figure 6 shows the surface velocity fields before and after interpolation. One can see that the interpolation onto a regular grid preserves the velocity field. To ensure that the velocity was correctly interpolated over land, node points were added in those regions and given velocities of zero for all time steps.

The FTLE computations presented below were performed by evaluating the derivatives in eq. 9 using finite differentiation. First, the node positions and boundary

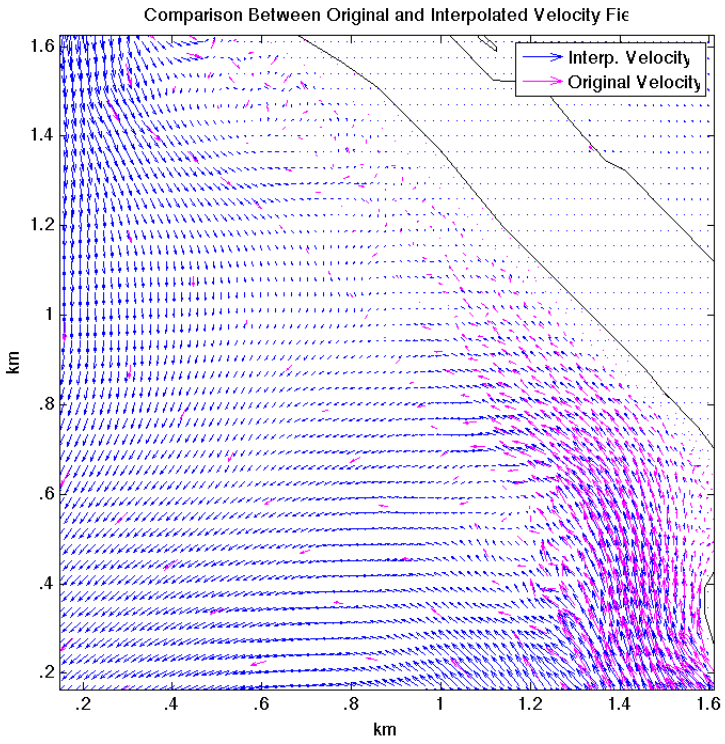

Figure 6: Pink: Original surface velocity field, computed from a triangular finite element grid. Blue: Surface velocity grid, computed after interpolation onto a regular grid.

points were defined in MANGEN (Manifold Generation). MANGEN was created by F. Lekien in order to calculate Lagrangian coherent structures (Lekien, 2007). The trajectory integrations involved in the FTLE computations were carried out using a time-step-adapting fourth/fifth-order Runge-Kutta method. The required spatiotemporal interpolations were performed using a linear method. The choice $\tau = 6$ hours was found sufficient to produce FTLE fields which unveil a good deal of attracting LCSs, which carry information about the future history of trajectories, and thus are most insightful for our purposes here. Longer time integration choices were found to result mainly in more detailed (attracting) LCSs without substantially affecting their position. The effects of the finite extent of the spatial domain on the FTLE calculations were minimized by performing the calculations over a domain much larger than that of interest.

Figure 7 shows a sequence of snapshots of the FTLE fields every 1.5 hours, produced using the surface velocity fields from the model for June 3rd 2010. The FTLE ridges (red indicates the highest separation rate) that are produced reveal attracting LCSs. The FTLE is the measure of maximum separation, so high FTLEs, computed backwards show maximum attraction. Due to the tidal influence on the circulation in the region, the FTLE fields primarily evolve periodically. Most of the LCSs are most apparent approximately every twelve hours, coinciding with the tidal period of the area. The most significant LCSs are those that are parallel and close to the shore, most apparent at 6:00, during high tide. These provide insight into the elevated levels of bacteria in the sand and intertidal zone, and why the identified non-point sources cannot alone account for the extreme concentrations of bacteria. One characteristic of an LCS is that there is no flux across them. These LCSs act as barriers to transport and mixing, inhibiting particles near the shore from being flushed away, so bacteria originating in the sand and intertidal zone remain for long periods of time, accumulating and reproducing. This is consistent with Shibata et al. (2004) findings

of maximum concentrations of indicator microbes during high tide, when the wash zone is under water.

LCSs are also present at the center of the coastline, running normal to the beach. These LCSs separate regions of fluid on the west and east sides of the beach and prevent mixing between them. Future research will look more closely to determine if these LCSs contribute to the retention of microbes on the beach and if there is a mathematical relationship between location along the coastline to the retention rate of passive tracers.

Black dots overlaid on the FTLE field shown in the 7th panel of 7 indicate points along FTLE ridges which belong on robust LCSs according to Haller (2011). The FTLE ridges were computed as attractors of the vector field $\boldsymbol{\nabla}\mathbf{F}_{t_0}^{t_0+\tau}(x_0)$ as proposed by Mathur et al. (2007). Verifying that a point on an FTLE ridge belongs on an LCS involves evaluating second-order spatial derivatives of the invariants of the Cauchy-Green tensor, which is difficult to achieve with precision. This diffculty explains why the FTLE ridges have not been possible to be completely covered by black dots. Note that most of the FTLE ridges, independent of their height, have black dots overlaid, which suggests that most of the FTLE ridges mark robust LCSs. These include, in particular, those FTLE ridges which take an along-shoreline orientation, which act as transport barriers for passive tracers released in their shoreward side.

Synthetic and satellite-tracked drifters were next used to verify the existence of the LCSs and investigate their effect on particle transport. By examining the FTLE fields, we can make several assumptions about what we will see in the drifter simulations: particles will be trapped along the coast; there will be little mixing between the right and left sides of water; and there will be an eddy formation on the west side of the beach.

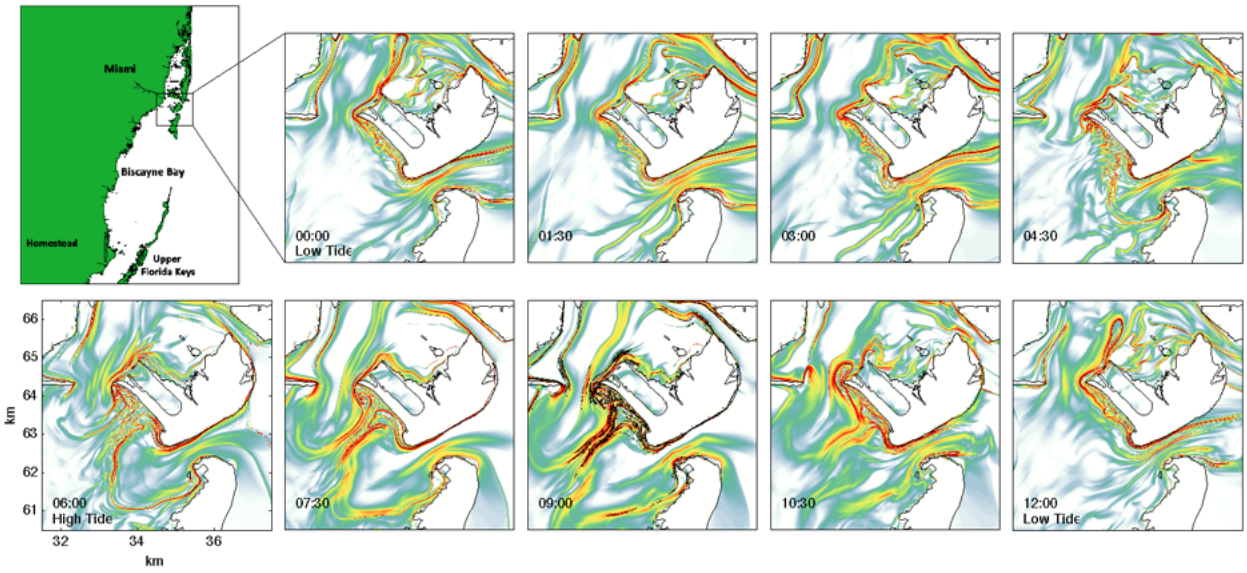

Figure 7: Sequence of snapshots of FTLE fields computed backward in time for June 3rd 2010. Ridges of the FTLE fields approximate attracting LCSs.

3.3 Simulated Drifters

Passively advected fluid particles were numerically simulated using surface velocities from the model. Figure 8 illustrates the effects that the LCSs have on particles that originate along the coast, shown in pink. These particles do not mix with surrounding fluid farther offshore, but remain above the LCS and stretch out around Virginia Key. This lack of mixing confirms the presence of LCSs as well the lack of transport across them, and thus, away from the shore. Any microbes that originate in the sand or water directly adjacent to the beach are trapped by the LCSs that run parallel to the shore. As the pink colored drifters are stretched and pushed in and out of the region, a large amount remains or continually returns. This drifter simulation agrees with predictions made using the FTLE fields, confirming that the FTLE ridges along the coastline are, in fact, LCSs.

The simulated drifters were also used to quantify the amount of fluid that becomes trapped in the area directly off the coast of Hobie Beach, as well as the length of time that must pass for the original fluid to be flushed out of the region. The bottom of

figure 8 shows the percentage of drifters that are located within the original starting area (the pink region in the first image) over time. One can see that peaks in concentration occur approximately every 12 hours, corresponding to the tidal cycle. After about 30 hours, 30 percent of the original drifters are still located in the original area. One could consider this to indicate that 30 percent of microbes introduced at $t_0 = 0$ will still remain in the area after 30 hours. This does not take into account any microbes put into the water at any other time. If all passive tracers put into the water along the coastline are retained at this rate, one can see that the number of microbes could become very high.

Figure 9 illustrates the effects that the LCSs have on mixing between the right and left sides of the beach. The orange, blue, and pink represent drifters on opposing sides of the FTLE lines running perpendicular to the beach that are present in Figure 7, and the cyan shows, again, the progression of drifters situated along the beach and inside an FTLE ridge running parallel to the coast. One can see the progression of the drifters along three hour intervals. After twenty hours, there is still little mixing between the left and right sides of water along Hobie Beach. This confirms that these ridges of the FTLE fields are LCSs and that they do serve as barriers to transport between one side and the other.

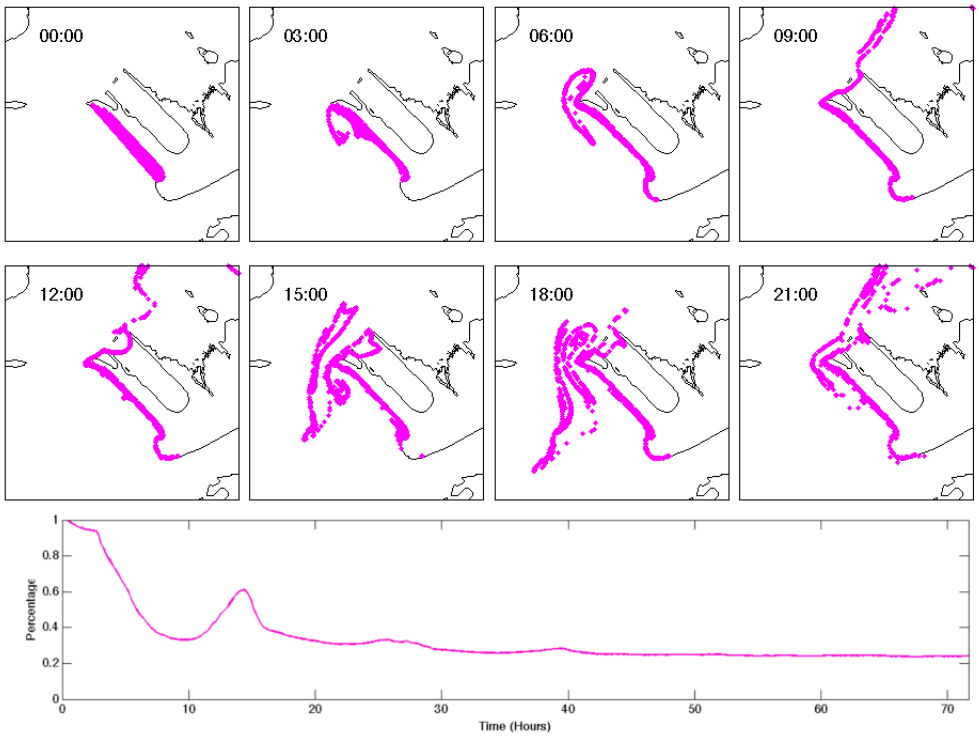

Figure 8: Top: Sequence of simulated drifters, 4 hour intervals. Bottom: Fraction of drifters originally located along the shore, that occupy the initial region over a period of 72 hours.

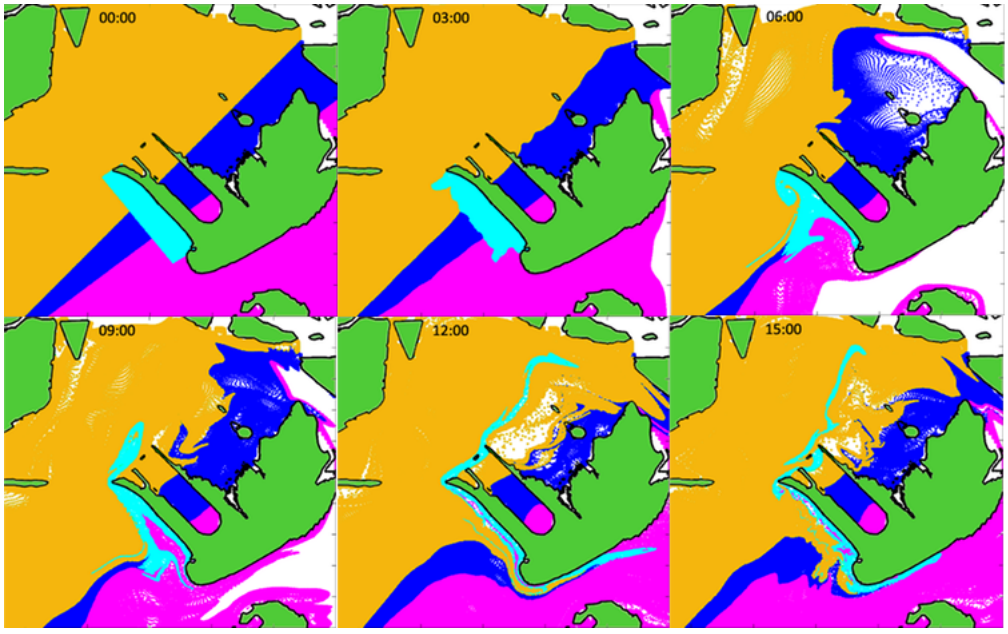

Figure 9: Sequence of simulated drifters, 3 hour intervals.

Chapter 4: Field Experimentation

4.1 Field Experiment 1: Method

In order to confirm the accuracy of the model results and the existence of Lagrangian coherent structures, an experiment was conducted using drifters in Biscayne Bay off of Hobie Beach. The drifters were mounted with Earthmate Blue Logger GPS devices to track their trajectories, as seen in Figure 10. These devices have been shown to provide valid Lagrangian estimates after some modifications (MacMahan et al., 2009). The drifters were released on June 3rd, 8th, and 11th for approximately 2 hours each. The trajectories recorded by the GPS devices were plotted and compared with drifter trajectories computed by MANGEN, as well as the FTLE fields.

Figure 10: Buoys equipped with GPS devices used to record fluid particle trajectories.

4.2 Field Experiment 1: Results

Figures 11 and 12 show results from June 3rd and 11th. The trajectories are plotted on instantaneous snapshots of FTLE fields. In figure 11, one can see that most of the LCSs are not present because the tide is low, but the ones that run parallel to the coastline remain. Although the water is moving away from the coast during this time, the drifters that are released between the FTLE ridges and the coast remain in the region. One can conclude that these FTLE ridges are LCSs, and that they act as

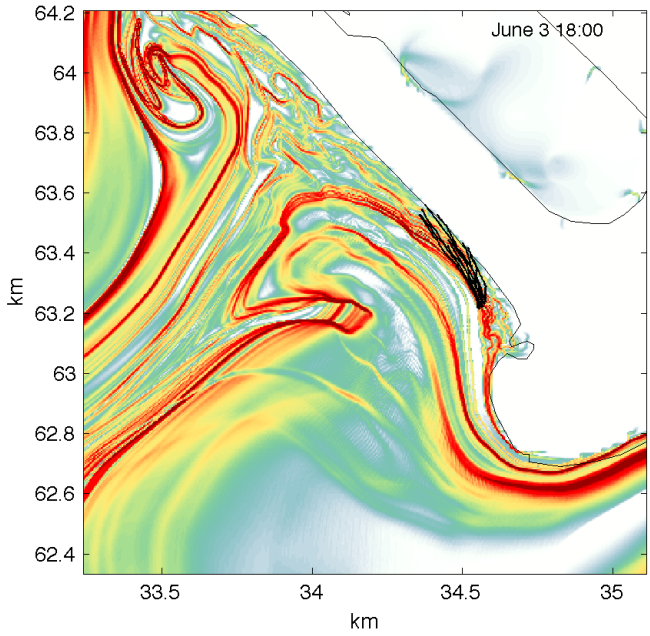

Figure 11: Experimental drifter trajectories recorded on June 3 2010 plotted on an instantaneous FTLE snapshot.

barriers to transport, trapping particles that originate along the coast. The drifters that were released on June 11th, on the eastern side of the beach, are attracted to the FTLE ridges in the center, and are then pushed away from the coast, never crossing the LCSs to the western side.

4.3 Field Experiment 2: Method

A second set of field experiments was designed, and consisted of tracking the trajectories of surface drifting buoys deployed in the vicinity of Hobie Beach. The drifters were constructed using off-the-shelf material and equipped with Locosys Technology GT-31 handheld GPS devices, as seen in figure 13. The GT-31 specifications state that it has an accuracy of 10m and 0.1m/s. These devices were chosen because they are water resistant and economical. Because the product was manufactured for water sports and not scientific research, in order to ensure their accuracy, they were compared with the Trimble GPS Total Station 4700, which has a 1cm horizontal and 2cm

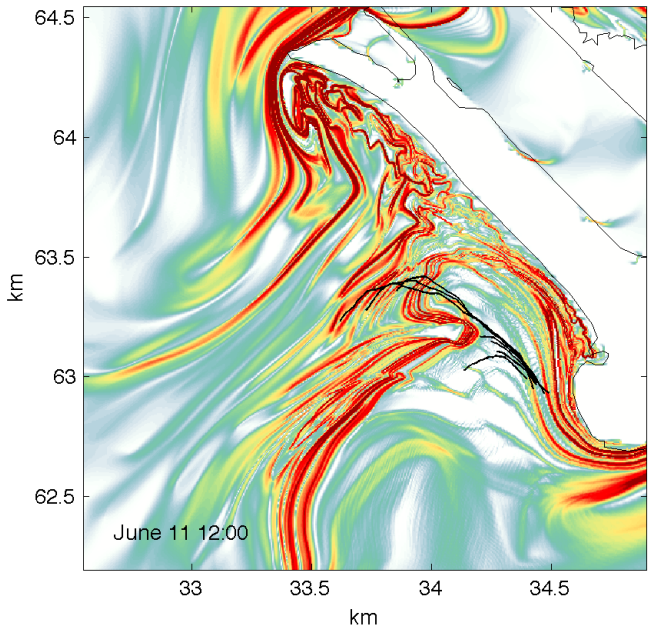

Figure 12: Experimental drifter trajectories recorded on June 11 2010, plotted on an instantaneous FTLE snapshot.

vertical accuracy. Both GPS systems were walked around Hobie beach, and the positions and velocities were compared. Figure 14 shows the differences in position and velocity between the two GPS devices at each point. The devices had a root mean square position difference of 8.2016m and a rms velocity difference of 0.2419m/s. These are acceptable results, because the CAFE3D model has a resolution of 15m near Hobie Beach.

4.4 Field Experiment 2: Results

The drifters were released on April 19th for approximately 3 hours. Figure 15 shows the trajectories from April 19th, plotted on a snapshot of the FTLE field at 14:00. One must remember that the FTLE field is an instantaneous snapshot at the end of the drifter trajectory, while the trajectory spans 3 hours. So, while it may seem that the drifters cross an LCS at the start, but in fact that LCS is not well defined at that moment. The trajectory does however show that it veers much farther to the

Figure 13: Left: Locosys GT-31 portable GPS; Middle: Drifter; Right: Drifters in Biscayne Bay off of Hobie Beach.

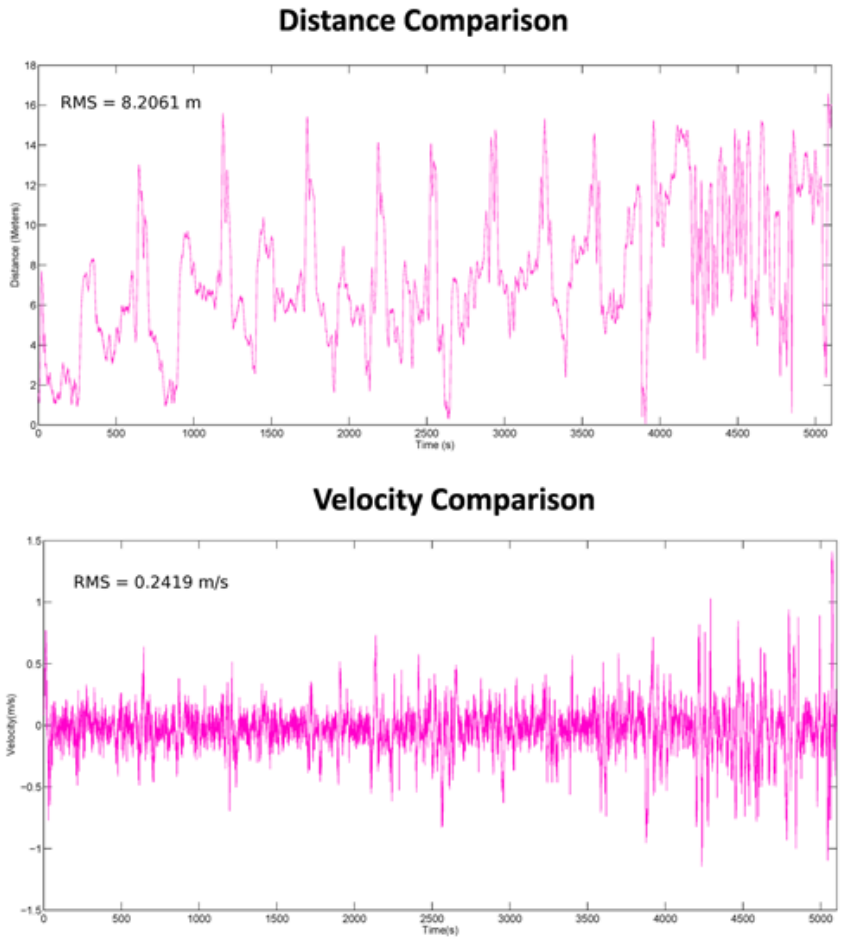

Figure 14: Position and velocity differences between GT-31 and Trimble GPS Total Station 4700.

left than the LCSs would suggest. The FTLE field on which these trajectories were plotted is one created using the surface velocities obtained from the model including wind.

The wind does not make a significant difference in the surface velocity fields nor the FTLE fields, but the drifters clearly follow a path that one would expect the wind cause. This indicates that the drifters are affected by the wind much more substantially than the water surface. Based on the construction of the drifter, it does not appear to have a high drag coefficient, but in order to determine the exact effect of the wind on the drifter itself, an experiment will soon be conducted in a wave tank. The drag coefficient can be approximated by finding the difference between the surface velocity and the drifter velocity, using wind as the only forcing mechanism on the water.

Figure 16 shows trajectories from April 8th 2011, 14:30 - 16:30, plotted on a snapshot of the FTLE field at 15:00. This experiment was conducted on a less windy day than on April 19th. One can see that the drifter trajectories are much more consistent with the LCSs, suggesting that the wind does have a large impact on the drifters. This experiment did not reveal much information because the drifters were released father south than intended, missing the eddy entirely. Also, drifters were released on the other side of the beach, but the GPS devices failed to record the trajectories due to human error.

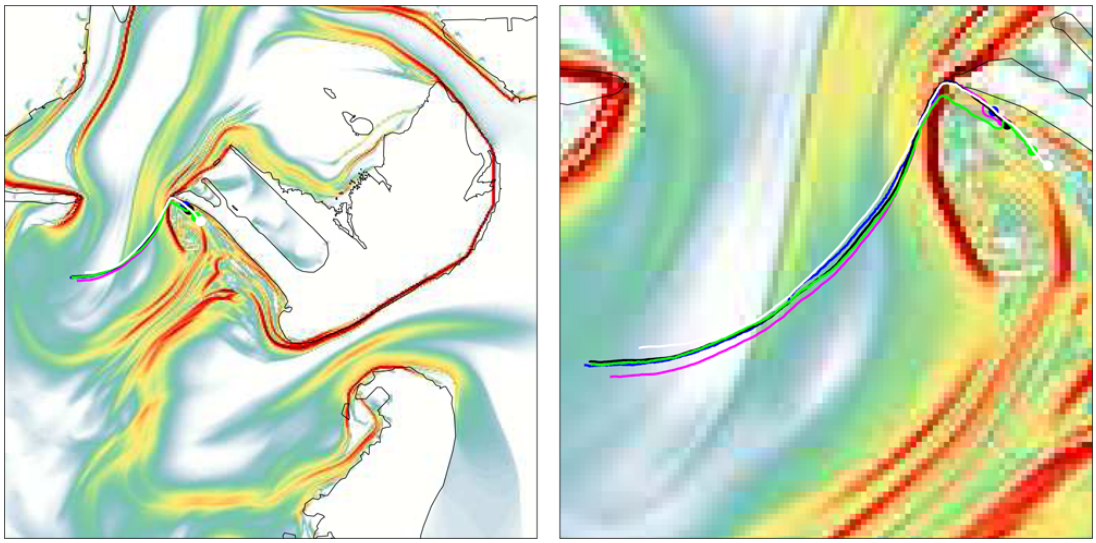

Figure 15: Experimental drifter trajectories recorded on April 19th 11:00 - 14:00, plotted on an instantaneous snapshot of the FTLE field at 14:00.

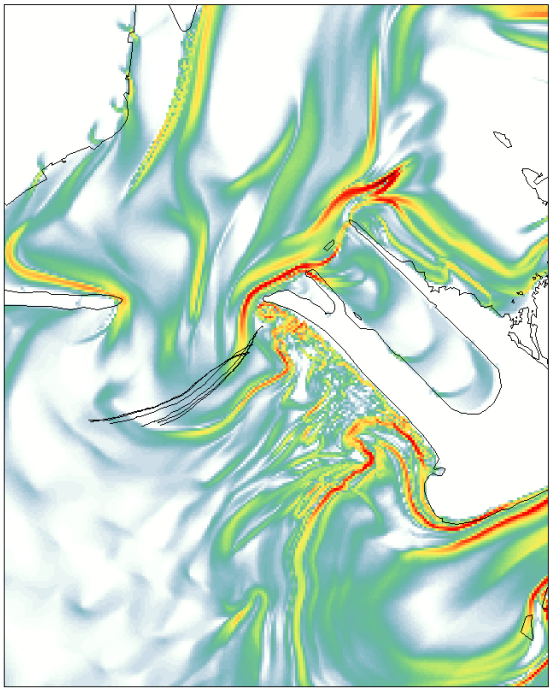

Figure 16: Experimental drifter trajectories recorded on April 8th 14:30 - 16:30, plotted on an instantaneous FTLE snapshots at 15:00.

Chapter 5: Discussion

An analysis of the coastal circulation at Hobie Beach was conducted using Lagrangian Coherent Structures in order to determine their role in the elevated levels of indicator bacteria in the area. Finite Time Lyapunov Exponents were calculated using the surface velocity fields produced from the hydrodynamic model CAFE3D. Numerically simulated drifter trajectories were also analyzed. Several experiments were conducted using GPS drifters in the water off Hobie Beach. These drifter trajectories were compared to the FTLE fields and simulated drifters to confirm the accuracy of the model results. From the drifter simulations, as well as field experiments, one can see that passive tracers are trapped in the area along the coastline by LCS. The Lagrangian circulation of Hobie Beach, influenced primarily by tide and land geometry causes a high retention rate of water near the shore, and can be used to explain the elevated levels of enterococci in the water.

Chapter 6: Future Work

The most immediate research will include experimentation on the new field drifters to determine their drag coefficient and accuracy in wind. Also, as shown in panel 7 of figure 7, more computations will be done to confirm which FTLE ridges are LCSs, as defined by Haller (2011)'s conditions in equation 12.

In the future, the coastal circulation of several other beaches will also be studied using Lagrangian Coherent Structures. Another beach at which dogs are permitted and is also tested by the Florida Department of Health under the Florida Healthy Beaches Program, is Canine Beach, located in Fort Lauderdale, FL at the intersection of Sunrise Blvd and A1A. This beach is similar to Hobie Beach in terms of climate, recreation, and the allowance of dogs, however, it does not have the same known water quality issues. Also part of the Healthy Beaches Program is Virginia Key Beach, located on the opposite side of Virginia Key from Hobie Beach. This beach, which does not allow dogs, is only about 1200 meters from Hobie Beach, but also does not have a recurring problem with water condition. The surface velocity fields for Canine Beach will need to be obtained. In order to use the surface velocity fields from the model already being used, the resolution will need to be increased to analyze the Virginia Key Beach. These locations will be studied and compared to Hobie Beach to determine the differences in coastal circulation that result in their lower microbe levels.

Finally, it will be helpful to locate a beach that is similar to Hobie Beach, including water quality, in order to determine the existence of Lagrangian coherent structures that act as transport controls and barriers in such a way as to trap pollutants, and to determine if the detection of such structures could be useful in explaining the cause of contaminated waters and in the prevention future problems in other locations around the world.

References

Apel, J. R. (1987). *Principles of Ocean Physics*. Academic Press.

Elmir, S. M., Wright, M. E., Abdelzaher, A., Solo-Gabriele, H. M., Fleming, L. E., Miller, G., Rybolowik, M., Shih, M.-T. P., Pillai, S. P., Cooper, J. A. and Quaye, E. A. (2007). Quantitative evaluation of bacteria released by bathers in a marine water. *Water Research* **41** (1): 3 – 10.

Haller, G. (2011). A variational theory of hyperbolic lagrangian coherent structures. *Physica D: Nonlinear Phenomena* **240** (7): 574–598.

Haller, G. and Yuan, G. (2000). Lagrangian coherent structures and mixing in two-dimensional turbulence. *Physica D: Nonlinear Phenomena* **147** (3-4): 352–370.

Lekien, F. (2007). Optimal pollution mitigation in monterey bay based on coastal radar data and nonlinear dynamics. *Environmental science and technology* **41** (18): 6562–6572, doi:10.1021/es0630691; pmid:.

MacMahan, J., Brown, J. and Thornton, E. (2009). Low-cost handheld global positioning system for measuring surf-zone currents. *Journal of Coastal Research* pp. 744–754, doi: 10.2112/08-1000.1; M3: doi: 10.2112/08-1000.1; 22.

Mathur, M., Haller, G., Peacock, T., Ruppert-Felsot, J. E. and Swinney, H. L. (2007). Uncovering the lagrangian skeleton of turbulence. *Phys. Rev. Lett.* **98** (14): 144502.

Olascoaga, M. J., Rypina, I. I., Brown, M. G., Beron-Vera, F., Koçak, H., Brand, L. E., Halliwell, G. R. and Shay, L. K. (2006). Persistent transport barrier on the west florida shelf. *Geophysical Research Letters* **33** (22): L22603.

Ottino, J. (1990). *The Kinematics of Mixing: Stretching, Chaos and Transport*. Cambridge University.

Shadden, S. C., Lekien, F. and Marsden, J. E. (2005). Definition and properties of lagrangian coherent structures from finite-time lyapunov exponents in two-dimensional aperiodic flows. *Physica D: Nonlinear Phenomena* **212** (3-4): 271–304.

Shibata, T., Solo-Gabriele, H. M., Fleming, L. E. and Elmir, S. (2004). Monitoring marine recreational water quality using multiple microbial indicators in an urban tropical environment. *Water Research* **38** (13): 3119 – 3131.

Streeter, V. L. (1961). *Handbook of Fluid Dynamics*. New York: McGraw-Hill.

Wang, J. D. (1978). Real-time flow in unstratified shallow water. *Journal of the Waterway Port Coastal and Ocean Division* **104** (1): 53–68.

Wang, J. D. and van de Kreeke, J. (1986). Tidal circulation in north biscayne bay. *Journal of Waterway, Port, Coastal, and Ocean Engineering* **112** (6): 615–631.

Wang, J. D., van de Kreeke Jacobus, Krishnan, N. and Smith, D. (1994). Wind and tide response in florida bay. *Bulletin of Marine Science* **54**.

Wiggins, S. (1992). *Chaotic Transport in Dynamical Systems*. Springer.

Wright, M. E., Solo-Gabriele, H. M., Elmir, S. and Fleming, L. E. (2009). Microbial load from animal feces at a recreational beach. *Marine pollution bulletin* **58** (11): 1649–1656.

Zhu, X. (2009). Modeling microbial water quality at a non-point source subtropical beach. Master's thesis, University of Miami.

Zhu, X., Wang, J. D., Solo-Gabriele, H. M. and Fleming, L. E. (2011). A water quality modeling study of non-point sources at recreational marine beaches. *Water Research* **45** (9): 2985 – 2995.